# Controlling Porosity of 3D Bioprinted Scaffold: A Process Parameter-Based Approach Abstract ID: 2252

Connor Quigley, Scott Clark, and MD Ahasan Habib\*

Sustainable Product Design and Architecture Department, Keene State College, Keene, NH 03435, USA.

## Abstract

Extrusion-based 3D bioprinting is a promising method for repairing patient-specific tissues and organs due to its inherent capacity to release biocompatible materials containing living cells in a preset area. The filament geometry and width mostly determine the scaffold architecture. Extrusion pressure, print speed, print distance, nozzle diameter, and material viscosity are just a few of the process variables that can be carefully chosen to affect the filament shape and width, ultimately verifying the user-defined scaffold porosity. To maintain defined filament width variation for various hydrogels within an acceptable range and to confirm the overall geometric fidelity of the scaffold, in this paper, filament width for a set of biomaterial compositions was determined using an image processing technique and an analytical relationship, including various process parameters, was developed.

# **Keywords**

3D bioprinting, prediction, regression model, printability, filament width.

## 1. Introduction

Using a computer-controlled 3D printing technique, the developing technology of "bio-printing" shows promises of reproducing 3D tissue scaffolds for tissue engineering [1, 2]. Compared to laser-assisted and inkjet bioprinting, extrusion-based bioprinting can deposit a wide range of materials, including heterogeneous bio-inks [3, 4]. With an incredibly straightforward method, acellular and cell-laden bio-ink have been extruded to construct scaffolds by altering the print parameters and resulted in good cell viability [5, 6]. The choice of biomaterial and its rheological and mechanical properties can directly impact the scaffolds created using the 3D bioprinting process [7-9]. Additionally, replicating the in-vivo microenvironment can encourage tissue growth by building scaffolds with regulated pore size, porosity, and pore connectivity [10]. Cell behavior within the scaffold structure is identified to be impacted by differences in pore size and geometry [11]. However, the extrusion-based bioprinting approach frequently shows a significant disparity between design and manufactured objects because of material and process attributes [12]. As a result, attaining shape fidelity, biocompatibility, and mechanical integrity within the scaffold structure can be challenging. Research is ongoing in pursuit of the best biomaterials to fabricate the 3D controlled porous structure utilizing additive manufacturing (bio-AM).

Natural hydrogels such as alginate, gelatin, chitosan, collagen, and fibrin are only a few examples that are frequently used to make scaffolds [13-15]. Along with those natural polymers, synthetic polymers such as polycaprolacton (PCL), polyethylene glycol (PEG), and polylactic acid (PLA) are employed in the 3D bioprinting process [15]. Alginate is usually chosen among them for the creation of scaffolds due to its biocompatibility and processability [24]. However, in order to achieve the desired shape fidelity and ensuing porosity of 3D printed scaffolds, we researchers primarily rely on the selection of the right material component and composition, leaving the choice of the right process parameters untested. Most of the time, the process parameters selection process is driven by the selection of materials [16, 17]. The specified scaffold architecture may not be printable due to unavailability of required process parameters such as air pressure, a 3D bioprinter with a wide range of capabilities, and nozzle size for a selected material. However, by systematically choosing a set of process parameters (PP), including nozzle diameter (ND), print speed (PS), print distance (PD), and extrusion pressure (EP), the filament geometry and width (FW) can be controlled. This can ultimately confirm the user-defined scaffold porosity of a material. For an example, if every process parameter considered constant, with increasing the applied pressure, the filament width will be increased as shown in Figure 1(a). In another scenario, selecting a set of systematic process parameters can ensure similar filament width as shown in Figure 1(b). To achieve defined scaffold structures with the resources at hand, there aren't enough analytical relationships between the printing process parameters and filament width. In order to maintain defined filament width variation for various hydrogels within an acceptable range and to confirm the overall geometric fidelity of the scaffold, in this paper, filament width was determined using an image processing technique and an analytical relationship, including various process parameters, was developed. With the help of suggested analytical relations, defined scaffold structures can be achieved.

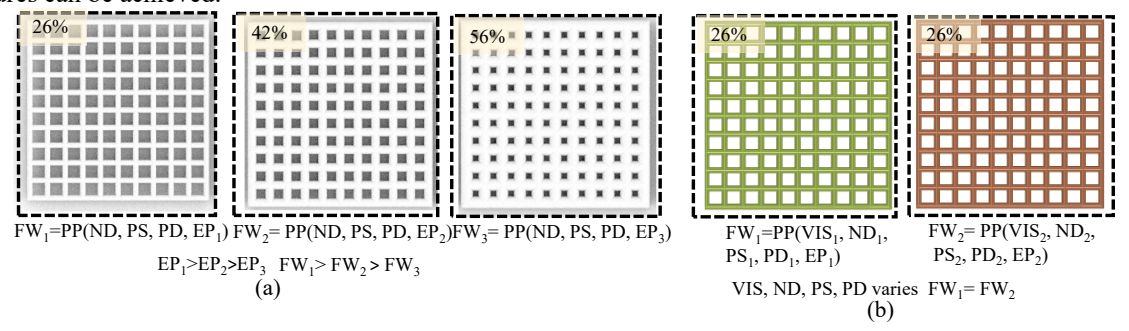


Figure 1: (a) Changes of filament width (FW) and subsequent porosities applying various extrusion pressures (EP) for a material maintaining nozzle diameter (ND), print speed (PS), print distance (PD) constant. here FW increases with ep, therefore, porosity reduces from 71% to 42% (b) similar FW with two different sets of pp for two different materials. porosity was determined by (total volume of scaffold-volume of solid) with respect to the total volume of the scaffold shown [18].

## 2. Materials and Methods

# 2.1 Material flow simulation

We used 4% (w/v) Alginate (w/v) (pH: 6.80) and 4% Carboxymethyl Cellulose (CMC) material (Sigma-Aldrich, St. Louis, MO, USA), in accordance with the procedure outlined in our prior research [24] to determine the effects of several process parameters, such as EP, PS, ND, and PD on the FW. In this paper, we will refer to this material composition as  $A_4C_4$ . The scaffolds and filaments were created using a 3D bio-printer that uses extrusion system called BioX (CELLINK, Boston, MA). In this research, s scaffold with 2 mm x 2 mm dimension including variable pore diameters, such as 2 mm x 8 mm and 8 mm x 8 mm was created.

Synthesized hydrogel was loaded in a 3.0 ml disposable nozzle, extruded pneumatically onto a fixed build plane. Rhino 6.0 (https://www.rhino3d.com), a visual basic-based CAD program, was used to create and specify the vectorized toolpath of a scaffold. A Bio-X compliant file containing the toolpath coordinates and all process parameters was created using Slicer (https://www.slicer.org), a G-code generation program, to build the scaffold. To fabricate the scaffold, the materials were dispensed on layers upon layers. Three filaments were created for each measurement. Using the CK Olympus bright field microscope, the photographs of manufactured filaments were obtained between one and two minutes after printing [25], and they were taken as quickly as feasible.

In this study, we employed PS as 5 and 15 mm/s, ND as 250 and 410  $\mu$ m to determine the effects of them on filament width. Throughout the studies, the print distance, z-height (ZH), bed temperature (BT), and print temperature (PT) were held constant at 150  $\mu$ m, 300  $\mu$ m, 23° C, and 30° C, respectively. All of them are listed in Figure 2(a). Process variables including layer height, print speed, and extrusion pressure were employed to manufacture the scaffold at 0.15 mm, 5 mm/s, and 110-120 kPa, respectively, to maintain the filament width identical for two distinct materials.

## 2.2 Analysis of the filament width

An image analysis technique was used to determine the filament's breadth. Within a minute of printing, final filament images were captured with a microscope as depicted in Figure 2. (b).

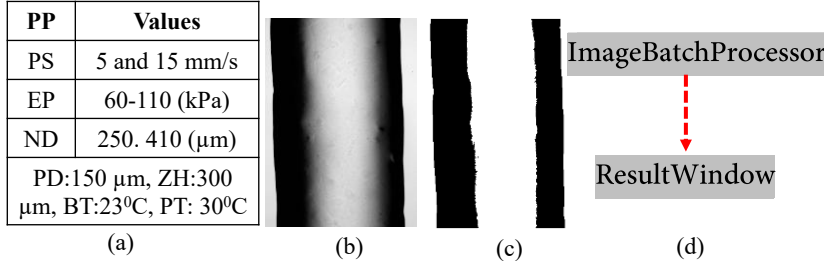


Figure 2: (a) List of process parameters used to fabricate filaments, (b) Images were taken of finished filaments with a microscope within a minute of printing (c) images were loaded into the program, processed and binarized, (d) utilizing image batch processing toolbox, and result window.

The MATLAB image batch processing toolkit (MATHWORKS, Natick, Massachusetts, USA) was used to examine. As illustrated in Figure 2(b), images were fed into the application, processed, and binarized before being measured across to get the width. The average width of the manufactured filament was then determined by repeating these measurements. In this research, the deviation between the actual filament width and the nozzle diameter was characterized as diffusion rate which as calculated by: (actual filament width-nozzle diameter)/nozzle diameterx100.

# 3. Results and discussions

### 3.1 Analysis of filament width

As illustrated in Figures 3, a total of 12 filaments were created using two nozzles with diameters of 250  $\mu m$  and 410  $\mu m$  utilizing various extrusion pressures and print speeds. Figure 4 (a) displays the extruded filament width for various applied pressures (60 kPa and 110 kPa) and print speeds (5 and 15 mm/s) through 250  $\mu m$  and 410  $\mu m$ . Figure 4(b) depicts a 3D surface plot for filament width for 410  $\mu m$  nozzle diameter with relation to print speeds and extrusion pressures.

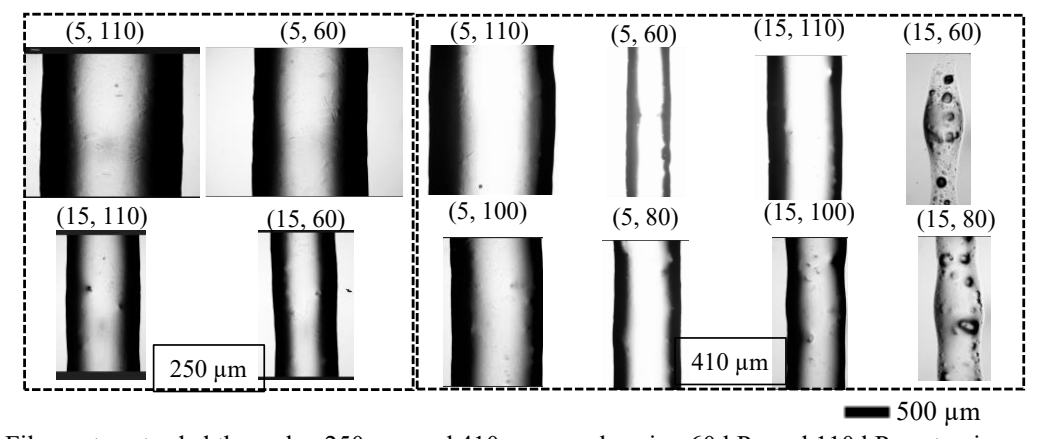


Figure 3: Filaments extruded through a 250  $\mu m$  and 410  $\mu m$  nozzle using 60 kPa and 110 kPa extrusion pressure and 5 mm/s and 15 mm/s print speeds.

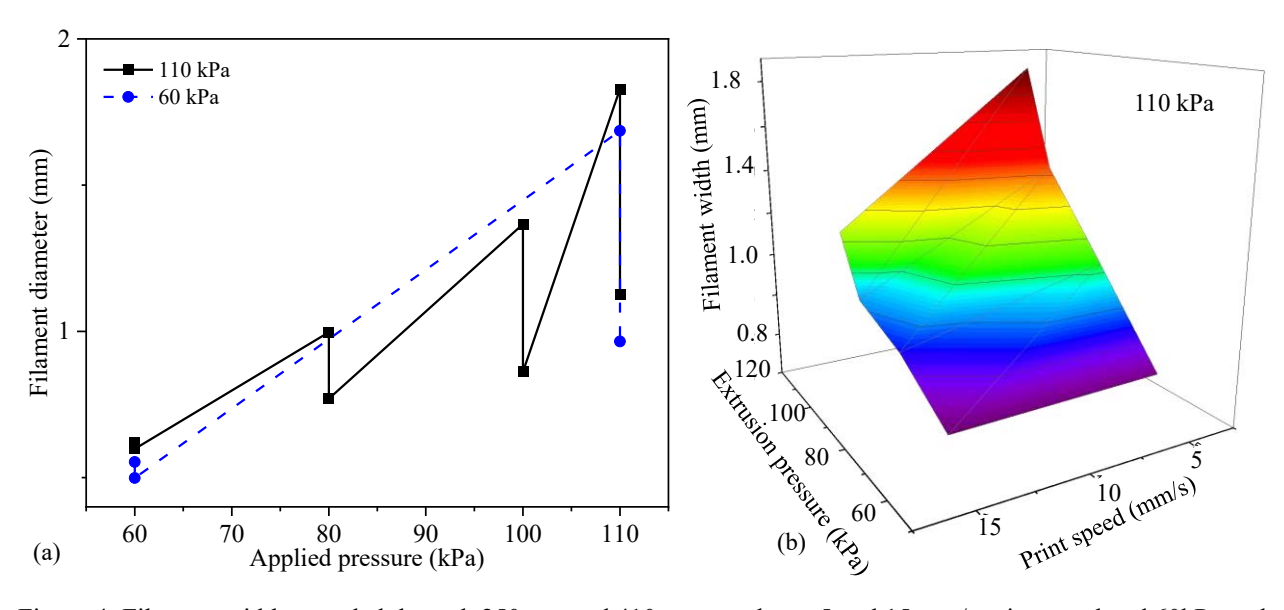


Figure 4: Filament width extruded through 250  $\mu$ m and 410  $\mu$ m nozzles at 5 and 15 mm/s print speed and 60kPa and 110 kPa extrusion pressure (b) a 3D surface plot representing filament width with respect to print speed and extrusion pressure for 410  $\mu$ m nozzle.

From Figure 4(a-b), it is clear that with increasing the extrusion pressure, the filament widths increase for both the nozzles. Since we only used  $A_4C_4$  as a sample material, to counteract the internal shear stress, same amount of extrusion pressures (either 60 or 110 kPa) drove higher number of materials released through larger 410  $\mu$ m nozzle. An as example, 83% elevation of extrusion pressure (from 60kPa to 110kPa), an 82% filament width increment observed released from 410  $\mu$ m nozzle. Two different values at the same extrusion pressure indicates that with increasing the print speeds, the filament widths reduced. Therefore, for every observation, the resultant filament width was larger by 5mm/s compared to the filament width for 15 mm/s print speed. An increment of 50% filament width extruded through 410  $\mu$ m nozzle at 110kPa is a proof of that observation.

We observed a similar filament width (0.55 mm and 0.59) showing a 7.4% difference fabricated with two different sets of process parameters such as (410 $\mu$ m, 60kPa, 15mm/s) and (250 $\mu$ m, 110kPa, 5mm/s). This interesting phenomenon indicates that we can achieve similar filament width by carefully selecting the available process parameters and resources. With an exhaustive search we found another similar filament width (0.96 mm and 0.99) showing even lower difference i.e., 3.2% with two different sets of process parameters such as (410 $\mu$ m, 80kPa, 5mm/s) and (250 $\mu$ m, 110kPa, 15mm/s). To demonstrate significance of the difference statistically, we conducted a two-sample t-test considering known variance and resulting p-value was 0.023(<0.05). Therefore, with a 95% confidence interval, we failed to reject the null hypothesis meaning they do not have significant differences. The difference we observed was due to random reasons.

## 3.2 Multiple regression

To determine an analytical relation between filament width and process parameters such as extrusion pressure, nozzle diameter, print speed, we used multiple linear regression methods. First, we conducted a multiple linear regression analysis for the filaments fabricated with 410µm and found the following relation:

$$FW = -0.027 + 0.016EP - 0.036PS \tag{1}$$

We observed the R- square value 85% meaning the relation we obtained can explain the 85% variance of the filament width can be described by variance of independent variables, extrusion pressure and print speed. However, the probability for interception was 0.94 for nozzle 410µm which is greater than the 0.15 meaning that interception is not significant to predict the filament width with respect to extrusion pressure and print speed. We then added nozzle diameter as third variable along with extrusion pressure and print speed and conducted multiple regression analysis to predict the filament with. We considered the following interactions: (EP, PS), (EP, ND), (PS, ND), and (EP, PS, ND) during the analysis and the resulted p-values were greater than 0.15 indicating they do not impact the filament width significantly.

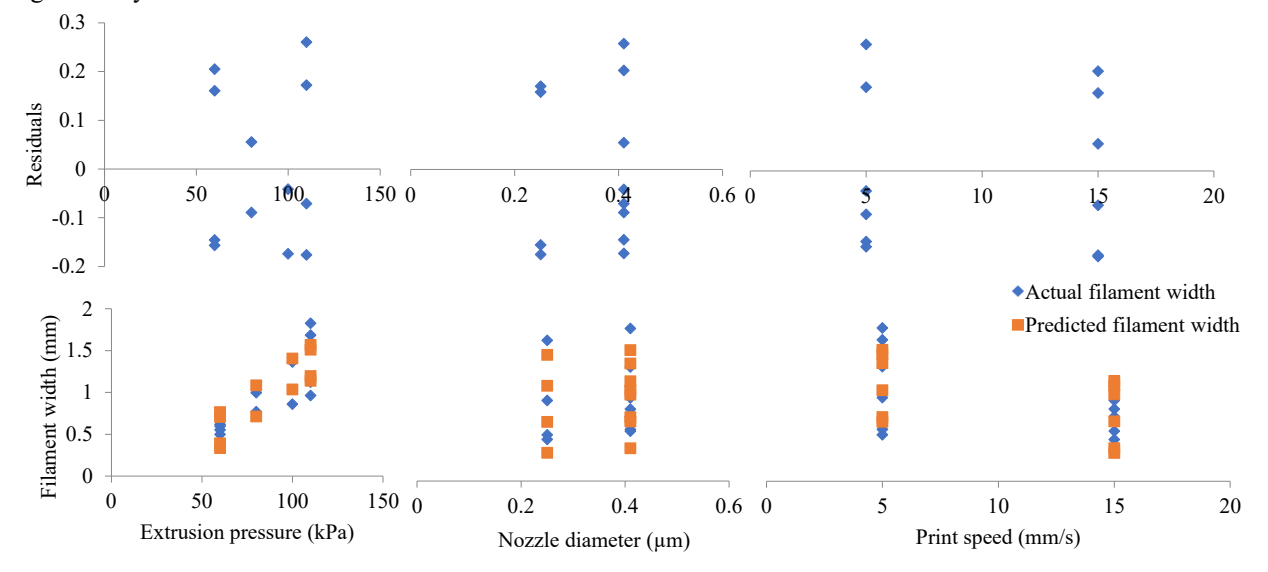


Figure 5: Prediction of filament width with residuals with respect to extrusion pressure, print speed, and nozzle diameter.

Therefore, we removed the interaction effect and conduct the regression analysis again and got the following relationship:

$$FW = -0.15 + 0.016EP - 0.037PS + 0.344ND \tag{2}$$

We observed the R- square value 86% meaning the relation we obtained can explain the 86% variance of the filament width can be described by variance of independent variables, extrusion pressure and print speed. However, the probability for interception was 0.67 for nozzle which is greater than the 0.15 meaning that interception is not significant to predict the filament width with respect to extrusion pressure and print speed. Figure 5 represents the residuals of the predicted filament width indicating a measure of how well the predicted filament width fits an individual data point. In this research, the residuals were distributed randomly and symmetrically across the mean line having a mean square error of 3.6%. The distribution of residuals does not show any pattern as well. Even though some data points show little distance from the mean line, others indicate that there is room to improve the model shown in Equation 2.

### 3.3 Analysis of filament width for various viscosities

In this section, material viscosity we added as another variable to analyze the filament width with existing process parameters mentioned in section 2.1.  $A_2C_6$ , another material along with  $A_4C_4$  was considered to demonstrate the controllability of filament (i.e., with similar width from two different materials) width by controlling the process parameters. Two scaffolds with variational pore sizes were fabricated following similar process parameters except 10kPa higher extrusion pressure for  $A_2C_6$  as shown in Figure 6. Since the viscosity of  $A_2C_6$  is higher than  $A_4C_4$  [19], the former material composition took higher extrusion pressure (120kPa) to maintain the filament width constant. Microscopic view presented only 5% variation of the filament width for scaffolds fabricated with  $A_2C_6$  and  $A_4C_4$ .

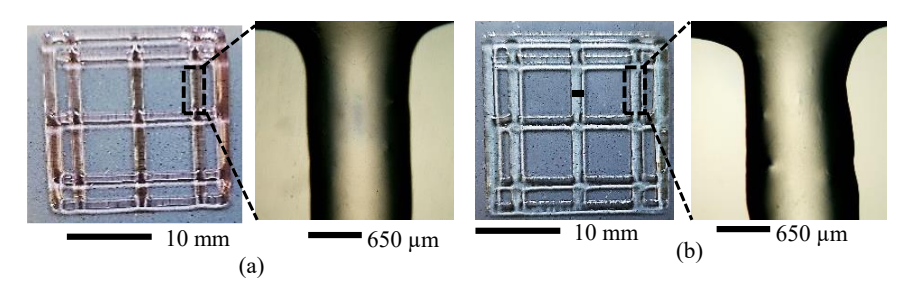


Figure 6: Scaffolds fabricated with (a)  $A_2C_6$  and (b)  $A_4C_4$  hydrogels with two different sets of printing parameters represents similar filament width.

## 4. Conclusion

The presented result clarifies that a systematic selection of process parameters can help fabricate scaffold with a defined filament width which eventually confirms the defined shape fidelity of the scaffold. The R-square value for a regression model predicting the filament width with respect to extrusion pressure, print speed, and nozzle diameter was identified 86%. We plan to include more experimental data to improve predictability of our proposed model in future. In addition to that, we plan to include the experimental data for nozzles of 200  $\mu$ m and 610  $\mu$ m maintaining similar extrusion pressure and print speeds. With an extensive number of experimental data, we also plan to explore a machine learning algorithm such Support Vector Machine (SVM) with increasing amount of experimental data to identify a strong predictive model so that we can fabricate defined filament width with available resources. Successfully achieving this long-term goal can take the extrusion-based 3D bioprinting technique one step ahead to fabricate patient-specific tissue scaffold.

## **Acknowledgements**

Research was supported by New Hampshire-EPSCoR through BioMade Award #1757371 from National Science Foundation and New Hampshire-INBRE through an Institutional Development Award (IDeA), P20GM103506, from the National Institute of General Medical Sciences of the NIH.

### References

- [1] C. Mandrycky, Z. Wang, K. Kim, and D.-H. Kim, "3D bioprinting for engineering complex tissues," *Biotechnology Advances*, vol. 34, no. 4, pp. 422-434, 2016/07/01/ 2016, doi: https://doi.org/10.1016/j.biotechadv.2015.12.011.
- [2] S. V. Murphy and A. Atala, "3D bioprinting of tissues and organs," *Nature biotechnology*, vol. 32, no. 8, pp. 773-785, 2014.
- [3] S. Ji and M. Guvendiren, "Recent advances in bioink design for 3D bioprinting of tissues and organs," *Frontiers in bioengineering and biotechnology*, vol. 5, p. 23, 2017.
- [4] K. Hölzl, S. Lin, L. Tytgat, S. Van Vlierberghe, L. Gu, and A. Ovsianikov, "Bioink properties before, during and after 3D bioprinting," *Biofabrication*, vol. 8, no. 3, p. 032002, 2016.
- [5] J. Jia et al., "Engineering alginate as bioink for bioprinting," Acta biomaterialia, vol. 10, no. 10, pp. 4323-4331, 2014.
- [6] L. Ouyang, R. Yao, Y. Zhao, and W. Sun, "Effect of bioink properties on printability and cell viability for 3D bioplotting of embryonic stem cells," *Biofabrication*, vol. 8, no. 3, p. 035020, 2016.
- [7] I. T. Ozbolat, A. Khoda, M. Marchany, J. A. Gardella, and B. Koc, "Hybrid tissue scaffolds for controlled release applications: A study on design and fabrication of hybrid and heterogeneous tissue scaffolds for controlled release applications is presented in this paper," *Virtual and Physical Prototyping*, vol. 7, no. 1, pp. 37-47, 2012.
- [8] K.-S. Han *et al.*, "Effect of pore sizes of silk scaffolds for cartilage tissue engineering," *Macromolecular Research*, vol. 23, no. 12, pp. 1091-1097, 2015.
- [9] A. Gottipati and S. Elder, "Effect of Chitosan Calcium phosphate Bead size on Scaffold Properties as they relate to Formation of Biphasic Constructs for Osteochondral Regeneration," *Journal of Polymer Materials*, vol. 34, no. 1, p. 287, 2017.
- [10] O. A. Hamid, H. M. Eltaher, V. Sottile, and J. Yang, "3D bioprinting of a stem cell-laden, multi-material tubular composite: An approach for spinal cord repair," *Materials Science and Engineering: C*, vol. 120, p. 111707, 2021.
- [11] C. M. Murphy, M. G. Haugh, and F. J. O'Brien, "The effect of mean pore size on cell attachment, proliferation and migration in collagen–glycosaminoglycan scaffolds for bone tissue engineering," *Biomaterials*, vol. 31, no. 3, pp. 461-466, 2010.
- [12] A. Khoda, I. T. Ozbolat, and B. Koc, "Engineered tissue scaffolds with variational porous architecture," *Journal of Biomechanical Engineering*, vol. 133, no. 1, p. 011001, 2011.
- [13] P. Erkoc *et al.*, "3D Printing of Cytocompatible Gelatin-Cellulose-Alginate Blend Hydrogels," *Macromolecular Bioscience*, vol. 20, no. 10, p. 2000106, 2020.
- [14] T. T. Demirtaş, G. Irmak, and M. Gümüşderelioğlu, "A bioprintable form of chitosan hydrogel for bone tissue engineering," *Biofabrication*, vol. 9, no. 3, p. 035003, 2017.
- [15] Y. She *et al.*, "3D Printed Biomimetic PCL Scaffold as framework interspersed with collagen for long segment tracheal replacement," *Frontiers in cell and developmental biology*, p. 33, 2021.
- [16] Z. M. Jessop *et al.*, "Printability of pulp derived crystal, fibril and blend nanocellulose-alginate bioinks for extrusion 3D bioprinting," *Biofabrication*, vol. 11, no. 4, p. 045006, 2019/07/08 2019, doi: 10.1088/1758-5090/ab0631.
- [17] A. Ribeiro *et al.*, "Assessing bioink shape fidelity to aid material development in 3D bioprinting," *Biofabrication*, 2017.
- [18] Q. L. Loh and C. Choong, "Three-dimensional scaffolds for tissue engineering applications: role of porosity and pore size," *Tissue Engineering Part B: Reviews*, vol. 19, no. 6, pp. 485-502, 2013.
- [19] C. Quigley, S. Tuladhar, and A. Habib, "A Roadmap to Fabricate Geometrically Accurate Three-Dimensional Scaffolds CO-Printed by Natural and Synthetic Polymers," *Journal of Micro-and Nano-Manufacturing*, vol. 10, no. 2, p. 021001, 2022.